Predictive analysis of *BRAF* V600E mutation and central lymph node metastasis in papillary thyroid carcinoma

JUNHUI PENG[1*], ZHIHUI WU[1*], YUJUN HUANG[2*], RUNHUA PAN[1], ZHONGDAI FU[3] and JIANZHANG WANG[4]

[1]Department of General Surgery, Shunde Hospital of Guangzhou University of Chinese Medicine, Foshan, Guangdong 528300, P.R. China;
[2]Department of Oncology, Shunde Hospital of Guangzhou University of Chinese Medicine, Foshan, Guangdong 528300, P.R. China;
[3]Department of Ultrasound, Shunde Hospital of Guangzhou University of Chinese Medicine, Foshan, Guangdong 528300, P.R. China;
[4]Department of Pathology, Shunde Hospital of Guangzhou University of Chinese Medicine, Foshan, Guangdong 528300, P.R. China

Received June 27, 2025; Accepted November 7, 2025

DOI: 10.3892/ol.2025.15397

Abstract. The incidence of thyroid carcinoma (THCA) has risen, yet most nodules remain indolent. In classical papillary thyroid carcinoma (PTC), central lymph node metastasis (CLNM) strongly impacts recurrence and survival, highlighting the need for accurate preoperative risk assessment. The present study aimed to identify clinical and molecular predictors of CLNM, focusing on the *BRAF* V600E mutation, and to develop a personalized nomogram. Gene expression profiles and clinical data from TCGA were analyzed to identify *BRAF* V600E-associated differentially expressed genes (DEGs) and construct a CLNM risk scoring model, which was further validated using retrospective preoperative fine-needle aspiration cytology (FNAC) and postoperative immunohistochemistry specimens. *BRAF* V600E was highly prevalent, and associated DEGs showed moderate discriminatory power. Multivariate analysis identified age, tumor size, and high-risk *BRAF* V600E status as independent predictors, integrated into a nomogram with an ROC of 0.710. Retrospective analyses confirmed the mutation's association with elevated CLNM risk. These findings suggest that patients with PTC with TI-RADS ≥4a nodules and no radiologic cervical LNM may benefit from combined preoperative evaluation, including *BRAF* V600E testing via FNAC, enabling precise CLNM risk stratification and supporting individualized surgical planning.

Correspondence to: Dr Zhihui Wu, Department of General Surgery, Shunde Hospital of Guangzhou University of Chinese Medicine, 12 Jinsha Avenue, Shunde, Foshan, Guangdong 528300, P.R. China
E-mail: wuzhgucm@163.com

*Contributed equally

Key words: papillary thyroid carcinoma, *BRAF* V600E mutation, central lymph node metastasis, nomogram, risk factor

Introduction

Thyroid carcinoma (THCA) is the fastest-growing malignancy globally, with papillary thyroid carcinoma (PTC) being the most prevalent subtype (1,2). Although PTC generally has a favorable prognosis due to its indolent nature, lymph node metastasis (LNM) in the neck can occur early, most often first affecting the central compartment. Central LNM (CLNM) is frequently identified only postoperatively, termed occult CLNM (3). In patients with PTC, cervical LNMs markedly increase the risk of recurrence and distant metastasis, making accurate preoperative assessment critical for determining the need for prophylactic central neck dissection (pCLND).

International guidelines recommend therapeutic lymph node dissection for patients with clinically evident central compartment metastasis (cN1 stage). However, the role of pCLND in patients with clinical lymph node negative (cN0) remains controversial. Japanese guidelines support routine pCLND, citing benefits in precise postoperative staging, treatment guidance and potential recurrence reduction (4). Conversely, the 2015 American Thyroid Association (5), 2019 European Society for Medical Oncology (6) and 2022 Chinese Anti-Cancer Association (7) guidelines advise pCLND only for cN0 patients with high-risk features, such as T3-T4 tumors, multicentricity, family history, childhood radiation exposure, or lateral cervical LNM. The 2022 National Comprehensive Cancer Network guidelines do not recommend routine pCLND (8). Although pCLND may decrease cervical lymph node recurrence by 34%, postoperative complication rates can reach 17.7% (9), highlighting the need for individualized preoperative assessment and predictive biomarkers for CLNM.

Currently, pCLND decisions rely heavily on surgical experience. Neck ultrasound, the primary imaging modality, has a sensitivity of only 15-40% for detecting CLNM, per the 8th edition of the AJCC manual (10-12). Computed tomography can be used as a supplement, however the indolent progression of PTC often limits detectable imaging changes associated with CLNM (13,14). Fine-needle aspiration cytology (FNAC) remains the most direct, accurate, and cost-effective preoperative diagnostic tool, enabling detection of molecular biomarkers such as *BRAF*, RAS and TERT

mutations. The *BRAF* V600E mutation, present in 40-80% of cases, is associated with aggressive PTC features. While some studies suggest it may predict CLNM in patients with cN0 (15), current evidence does not support using *BRAF* V600E alone to guide pCLND. Integrating additional indicators may enhance predictive accuracy and inform surgical planning (16,17).

To elucidate the relationship between *BRAF* V600E, clinicopathological features and CLNM in PTC, the present study analyzed gene expression profiles and clinical data from The Cancer Genome Atlas (TCGA) and the Gene Expression Omnibus (GEO) databases. It aimed to develop a risk scoring model for CLNM based on differentially expressed genes (DEGs) stratified by *BRAF* V600E status. Furthermore, patients with cN0 PTC treated at the General Surgery Department of Shunde Hospital of Guangzhou University of Chinese Medicine (GUCM) were included, with preoperative CLNM tissues collected via ultrasound-guided FNAC and postoperative thyroid tissue analyzed for *BRAF* V600E. The present study sought to support personalized preoperative assessment, optimize surgical decisions, reduce unnecessary lymph node dissection and improve postoperative quality of life.

Materials and methods

Public data collection and processing. mRNA expression profiles and clinical data for THCA patients were obtained from TCGA database. Level 3 HTSeq-FPKM data were normalized to transcripts per million reads. For external validation, GSE60542 and GSE29265 datasets were retrieved from the Gene Expression Omnibus (https://www.ncbi.nlm.nih.gov/geo/).

Tumor mutation analysis. The prevalence of *BRAF* mutations across cancer types was initially assessed using cBioPortal (http://www.cbioportal.org). Somatic mutation data from TCGA were analyzed with the R package 'maftools' to visualize mutation frequencies and types, focusing on THCA. After confirming *BRAF* V600E as the predominant mutation in THCA, samples harboring this mutation and their associated clinical data were downloaded from cBioPortal for further analysis.

DEGs' analysis. Data of patients with THCA obtained from TCGA were stratified into *BRAF* V600E mutant and wild-type groups. Differential expression analysis was performed using the R package limma 3.52.2 (18). DEGs were defined by an adjusted P-value <0.05 and |log2-fold-change (FC)|>1.5.

Functional enrichment analysis. To explore the biological significance of DEGs, Gene Ontology (GO) and Kyoto Encyclopedia of Genes and Genomes (KEGG) pathway analyses were conducted using the ClusterProfiler R package 4.4.4 (18).

Construction and validation of the diagnostic risk model. A diagnostic risk model for predicting CLNM in THCA was established using DEGs from both *BRAF* V600E mutant and wild-type cases via Lasso-Cox regression with the glmnet package 3.0 (glmnet.stanford.edu/). The model was formulated as:

$$Risk\ score = \sum_i (coefi \times expi)$$

where 'expi' denotes gene expression and 'coefi' represents the corresponding gene risk coefficient. Model performance was evaluated using Receiver Operating Characteristic (ROC) and Precision-Recall (PR) curves. External validation was performed using the GSE60542 and GSE29265 datasets.

It should be noted that genes such as CST6 and LOX were included solely as part of the predictive model, and their downstream mechanistic roles in CLNM were not experimentally investigated in the present study, representing a limitation.

Immune infiltration analysis. The relative enrichment of 24 immune cell types in THCA was assessed using single-sample Gene Set Enrichment Analysis (ssGSEA) *via* the R package GSVA 3.19 (19). Spearman's correlation analysis was performed to evaluate associations between the risk score and immune cell infiltration. P-values from the 24 parallel tests were adjusted using the Benjamini-Hochberg false discovery rate (FDR), with significance defined as FDR<0.05. Differences in immune infiltration between high- and low-risk groups were analyzed using the Wilcoxon rank-sum test. Additionally, immune, stromal and ESTIMATE scores were calculated using the ESTIMATE algorithm (20).

The correlation between the risk score and expression of interleukins, chemokines and immune checkpoints was further examined. Immunophenoscore (IPS) was used to predict potential responses to immunotherapy (anti-PD-1 and anti-CTLA-4) based on gene expression profiles, leveraging data from The Cancer Immunome Atlas (https://tcia.at/).

Construction and validation of the nomogram. A binary logistic regression model was constructed using the glm function in R to predict overall survival probability. The RMS package was used to develop and visualize the nomogram. Calibration curves and restricted cubic spline plots were employed to evaluate the nomogram's performance. The concordance index (C-index) quantified its discriminative ability and decision curve analysis was performed to assess net clinical benefit.

Retrospective analyses of pathological samples

Preoperative assessment of BRAF V600E mutation in central lymph nodes via PCR. Clinical data and ultrasound-guided FNAC results were collected from 32 patients with cN0 PTC who underwent preoperative assessment at Shunde Hospital of GUCM between August 2022 and November 2023 (Foshan, China). Inclusion criteria were: i) FNAC-confirmed or highly suspected PTC with TI-RADS 5 nodules; ii) No LNM on preoperative ultrasound/CT, classified as cN0 per Kowalski criteria; iii) Central lymph node diameter >0.5 cm. Exclusion criteria included prior thyroid surgery, history of thyroid disease treatments (including I-131 therapy), and incomplete clinical data. FNAC was performed by an experienced physician, and the specimens were sent to Guangzhou Da'an Clinical Laboratory for BRAF V600E mutation detection

using ARMS-PCR (cat. no. 56404 LOT:026ABB01; Wuxi Shenrui Bio-Pharmaceuticals Co. Ltd.).

Postoperative immunohistochemical (IHC) analysis of BRAF V600E mutation. Clinical and pathological data from 222 patients with PTC treated between January 2022 and November 2023 were collected. Inclusion criteria were: i) age ≥18 years; ii) histologically confirmed PTC; and iii) first diagnosis of THCA. Exclusion criteria included incomplete data, non-primary THCA, or presence of other malignancies. Collected variables included age, sex, histopathological subtype, tumor location and size, central lymph node status, IHC results, and surgical approach. CLNM was independently assessed by two blinded pathologists to minimize observer bias. IHC was used to detect *BRAF* V600E protein expression, with positivity determined by staining intensity and cytoplasmic localization.

Ethics statement. The present study was approved by the Ethics Committee of Shunde Hospital of Guangzhou University of Chinese Medicine (approval nos. KY2022066 and KY2023127; Foshan, China). All procedures were performed in accordance with relevant guidelines and regulations.

Statistical analysis. Group differences were evaluated using the Wilcoxon test. Associations between categorical variables were assessed using the Chi-squared test or Fisher's exact test, as appropriate; Fisher's exact test was applied when more than 20% of the cells in a contingency table had an expected count of less than 5. Spearman correlation analysis was used to examine associations between risk score and immune infiltration. $P<0.05$ was considered to indicate a statistically significant difference, with multiple testing corrections applied using the Benjamini-Hochberg FDR method.

Results

Characteristics of the TCGA cohort. A total of 508 TCGA patients pathologically diagnosed with PTC with available clinical and RNA-sequencing data were analyzed. Among these, 490 samples had documented *BRAF* mutation status and were included in further analyses. Clinicopathological characteristics of the cohort are summarized in Table I.

BRAF genetic variations in the TCGA cohort. The mutational landscape of *BRAF* was analyzed across 10,967 samples from 32 cancer types using cBioPortal. THCA exhibited the highest *BRAF* mutation frequency, accounting for 59.6% of cases (Fig. 1A). Examination of THCA mutations, illustrated by a waterfall plot (Fig. 1B), showed that missense mutations were predominant (77.73%). Analysis of 284 mutation sites across amino acids 0-766, including one duplicate, confirmed that *BRAF* V600E mutations were exclusively missense (Fig. 1C). Chi-squared analysis revealed a significant association between *BRAF* V600E and CLNM. The mutation group exhibited a CLNM rate of 59.1%, significantly higher than 35.7% in the non-mutation group (Fig. 1D). A Sankey diagram (Fig. 1E) further illustrated the strong link between *BRAF* V600E mutations and higher CLNM incidence, whereas the non-mutation group displayed minimal CLNM.

Identification of DEGs in THCA. A total of 229 DEGs were identified between *BRAF* V600E mutant and wild-type groups, including 57 upregulated (24.9%) and 172 downregulated genes (75.1%), using thresholds of adjusted $P<0.05$ and $|\log2\text{-FC}|>1.5$ (Fig. 2A and B; Table SI).

KEGG pathway analysis indicated that upregulated genes were significantly enriched in 'thyroid hormone synthesis, thyroid hormone signaling and Rap1 signaling pathways (Fig. 2C). GO analysis showed enrichment in thyroid hormone metabolism, hormone generation, and metal ion stress response processes (Fig. 2D). By contrast, downregulated genes in the non-*BRAF* V600E group were associated with KEGG pathways including viral myocarditis, type I diabetes mellitus, and toxoplasmosis (Fig. 2E). GO analysis highlighted their involvement in regulating monocyte, lymphocyte and leukocyte proliferation (Fig. 2F).

Development and validation of a diagnostic model using DEGs. Based on the identified association between *BRAF* V600E mutation and CLNM (Fig. 3A and B), the authors evaluated whether the 229 DEGs could serve as a diagnostic signature. Lasso regression was used to construct a risk score model:

$$Risk\ score = (0.028 \times CST6) + (-0.026 \times MT1G) + (0.004 \times CLDN10) + (-0.034 \times SOD3) + (-0.018 \times KCNAB1) + (0.123 \times LOX) + (0.113 \times SCEL) + (-0.003 \times C3)$$

This model stratified THCA samples into high- and low-risk groups and achieved a ROC AUC of 0.710 (95% CI: 0.664-0.755), indicating acceptable accuracy (Fig. 3C and D). External validation in GEO datasets yielded ROC AUCs of 0.666 (95% CI: 0.542-0.791) in GSE60542 and 0.905 (95% CI: 0.683-1.0) in GSE29265, demonstrating moderate to high predictive performance (Fig. 3E-H).

Incorporation of CLNM status showed significantly higher risk scores in the N1 group, reflecting elevated CLNM rates in high-risk samples (Fig. 4A). Analysis of *BRAF* V600E-related signature genes revealed that CST6, CLDN10, LOX, and SCEL were upregulated in the LNM group, whereas MT1G, SOD3, and KCNAB1 were higher in the N0 group (Fig. 4B). Individual gene ROC AUCs for LNM prediction were: CST6 (0.64), MT1G (0.657), CLDN10 (0.647), SOD3 (0.648), KCNAB1 (0.645), LOX (0.661), SCEL (0.657) and C3 (0.549), indicating moderate discriminative ability (Fig. 4C).

Association between risk score and immune landscape. The relationship between risk scores and the immune landscape in THCA were evaluated by comparing immune cell composition between low- and high-risk groups. ssGSEA demonstrated a strong positive correlation ($R>0.5$) between risk score and multiple immune cell types, including dendritic cells (DCs), macrophages, immature DCs (iDCs), Th1 cells, neutrophils, Treg cells, and Th2 cells, with significance maintained after Benjamini–Hochberg FDR correction (Fig. 5A). High-risk samples exhibited higher proportions of these immune cells (Fig. 5B), as well as elevated ESTIMATE, stromal and immune scores (Fig. 5C-E), indicating increased immune infiltration.

Analysis of the tumor immune microenvironment revealed that most interleukins, except IL12A, IL17D and IL34, were upregulated in the high-risk group (Fig. 5F). Similarly,

Table I. Clinical pathological characteristics of patients with papillary thyroid carcinoma from TCGA.

Characteristic	Overall, no. (%)	*BRAF* V600E		P-value
		Mut, no. (%)	Non-mut, no. (%)	
n	508	285	205	
Sex (%)				0.822
Female	371 (73.2)	208 (73.2)	152 (74.1)	
Male	136 (26.8)	76 (26.8)	53 (25.9)	
Age, n (%)				0.772
≤45	239 (47.1)	152 (53.5)	107 (52.2)	
>45	268 (52.9)	132 (46.5)	98 (47.8)	
Pathologic T stage, n (%)				0.001
T1	144 (28.5)	17 (6)	5 (2.5)	
T2	167 (33.1)	79 (27.9)	82 (40.2)	
T3	171 (33.9)	76 (26.9)	64 (31.4)	
T4	23 (4.6)	111 (39.2)	53 (26)	
Pathologic N stage, n (%)				<0.001
N0	231 (50.5)	155 (59.2)	63 (35.2)	
N1	226 (49.5)	107 (40.8)	116 (64.8)	
Pathologic M stage, n (%)				0.735[a]
M0	283 (96.9)	170 (97.1)	104 (96.3)	
M1	9 (3.1%)	5 (2.9)	4 (3.7)	
Pathologic stage, n (%)				<0.001
Stage I	285 (56.4)	38 (13.4)	15 (7.4)	
Stage II	52 (10.3)	18 (6.4)	32 (15.7)	
Stage III	113 (22.4)	152 (53.7)	122 (59.8)	
Stage IV	55 (10.9)	75 (26.5)	35 (17.2)	
Ethnicity (%)				0.478
Asian and Black or African American	80 (19.3)	45 (18.3)	32 (21.2)	
White	334 (80.7)	201 (81.7)	119 (78.8)	
Histological type, n (%)				<0.001
Classical	359 (77.9)	232 (93.9)	111 (56.3)	
Follicular	102 (22.1)	15 (6.1)	86 (43.7)	
Residual tumor (%)				0.113[*]
R0	389 (87.4)	215 (85)	163 (91.6)	
R1	52 (11.7)	35 (13.8)	14 (7.9)	
R2	4 (0.9)	3 (1.2)	1 (0.6)	
Primary neoplasm focus type, n (%)				0.551
Multifocal	228 (45.9)	149 (53)	111 (55.8)	
Unifocal	269 (54.1)	132 (47)	88 (44.2)	
Neoplasm location, n (%)				0.158
Bilateral	86 (17.2)	111 (39.5)	97 (48%)	
Isthmus	22 (4.4)	102 (36.3)	70 (34.7)	
Left lobe	178 (35.5)	52 (18.5)	29 (14.4)	
Right lobe	215 (42.9)	16 (5.7)	6 (3)	
Thyroid gland disorder history (%)			0.047	
Lymphocytic Thyroiditis	72 (16.1)	12 (4.8)	12 (6.6)	
Nodular Hyperplasia	69 (15.4)	31 (12.4)	35 (19.2)	
Normal	281 (62.7)	36 (14.3)	34 (18.7)	
Other, specify	26 (5.8)	172 (68.5)	101 (55.5)	

Categorical data are presented as n (%).[a]P-values were obtained using Fisher's exact test (Monte Carlo method, based on 10,000 sampled tables) due to the presence of expected cell counts <5.

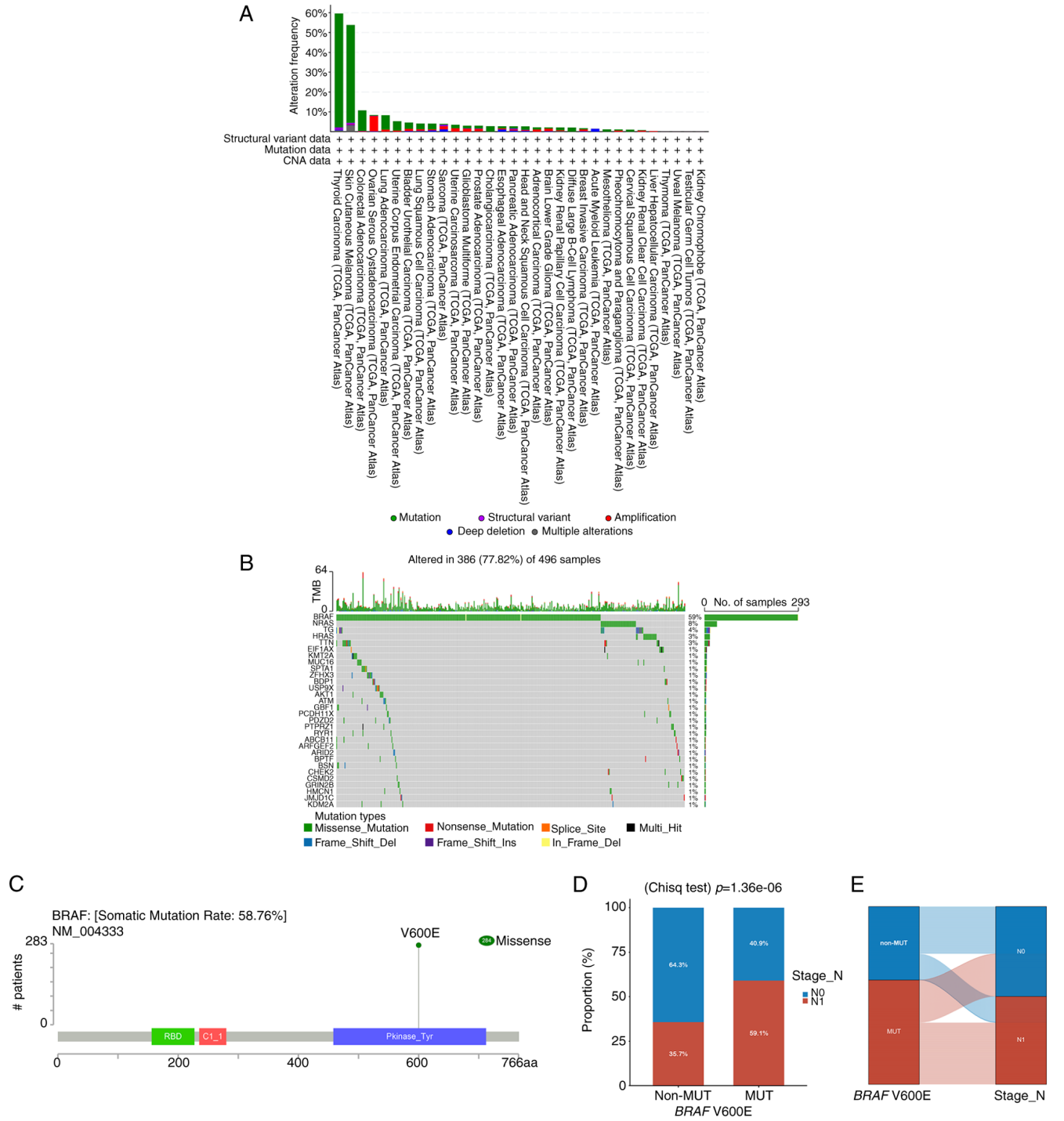

Figure 1. Landscape of *BRAF* mutations and CLNM in PTC. (A) Pan-cancer distribution of *BRAF* mutations across 32 tumor types in TCGA, with THCA showing the highest frequency. (B) Waterfall plot of *BRAF* mutation types in THCA, highlighting predominance of missense mutations. (C) Lollipop plot showing amino acid mutation positions in THCA; V600E is the most frequent variant. (D) CLNM incidence comparison between *BRAF* V600E mutant and wild-type patients (P<0.001). (E) Sankey diagram illustrating the relationship between *BRAF* V600E mutation status and CLNM occurrence. CLNM, central lymph node metastasis; PTC, papillary thyroid carcinoma; THCA, thyroid carcinoma; TCGA, The Cancer Genome Atlas.

chemokines and their receptors were generally elevated, except for CCL16, CCL25 and CCR10 (Fig. 5G). Immune checkpoint analysis showed higher expression of inhibitory molecules, including BTLA, CD244, CD274, CSF1R, CTLA4, HAVCR2, IL10, KDR, LGALS9, PDCD1LG2, TGFβ1, TGFβR1, TIGIT and VTCN1, in the high-risk group (Fig. 6A), alongside increased levels of most stimulatory checkpoint molecules (Fig. 6B). These findings suggest that high-risk THCA patients exhibit enhanced immune infiltration with both inhibitory and stimulatory components, highlighting potential responsiveness to immunotherapy.

Finally, IPS were higher in the high-risk group across CTLA4-negative PD-1-positive, CTLA4-positive PD-1-negative, and CTLA4-positive PD-1-positive conditions (Fig. 6C-F), indicating a more active and potentially immunotherapy-responsive tumor microenvironment (TME).

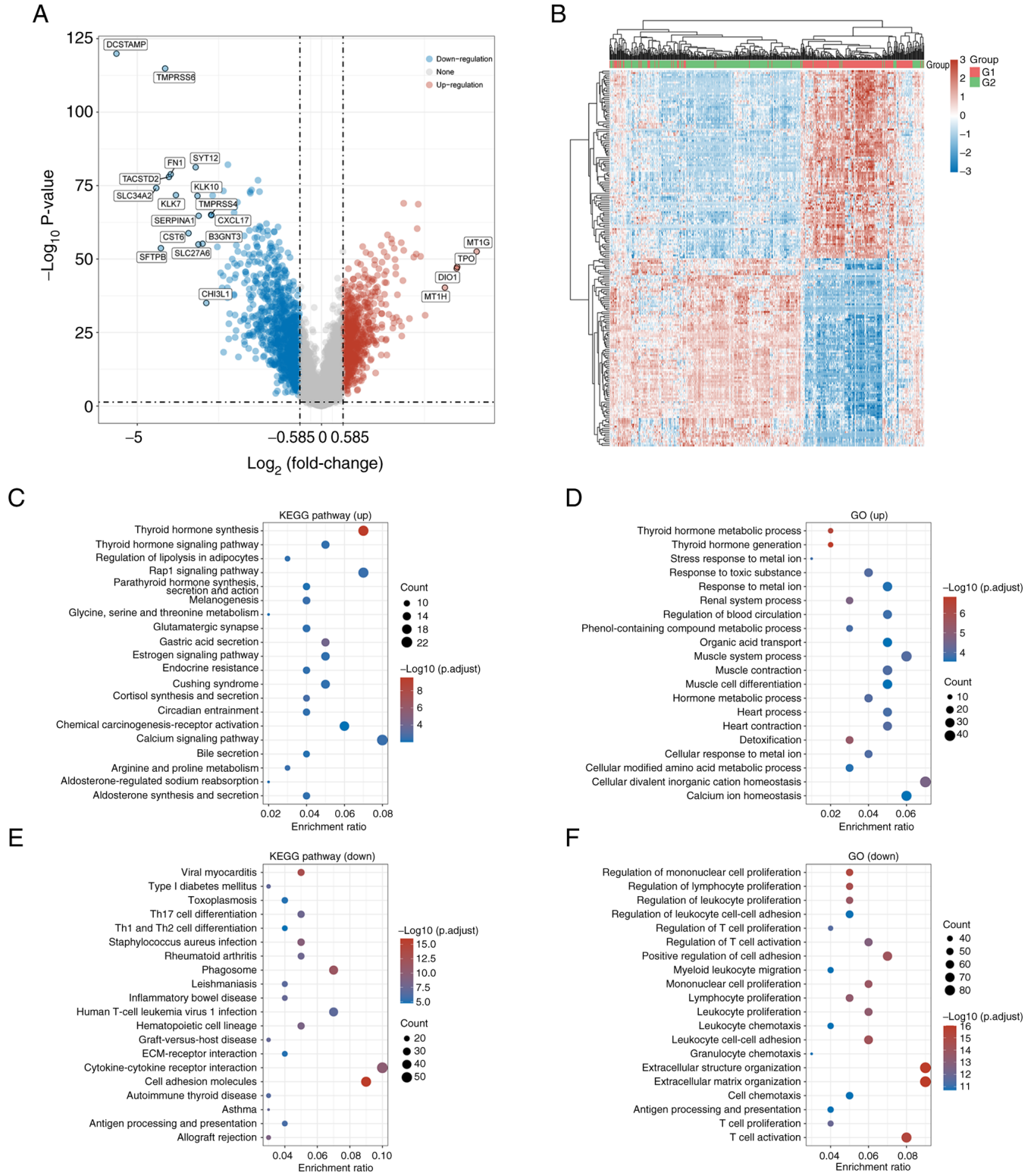

Figure 2. Differential gene expression and functional enrichment in *BRAF* V600E PTC. (A) Volcano plot showing significantly up- and downregulated genes between *BRAF* V600E mutant and wild-type tumors. (B) Heatmap of top DEGs stratified by mutation status. (C and D) KEGG and GO enrichment analyses of upregulated genes highlighting thyroid hormone biosynthesis and stress response pathways. (E and F) KEGG and GO enrichment analyses of downregulated genes implicating immune regulation and infection-related pathways. DEGs, differentially expressed genes; KEGG, Kyoto Encyclopedia of Genes and Genomes; GO, Gene Ontology.

Nomogram development for risk score in independent diagnostic analysis. Logistic regression analysis of TCGA clinical data identified several factors significantly associated with increased CLNM risk: age (HR=2.032, 95% CI: 1.298-3.179), T2 stage (HR=1.902, 95% CI: 1.086-3.331), T3 stage (HR=2.709, 95% CI: 1.555-4.719), T4 stage (HR=12.940, 95% CI: 3.309-50.602), and risk score (HR=3.910, 95% CI: 2.518-6.071; Table II).

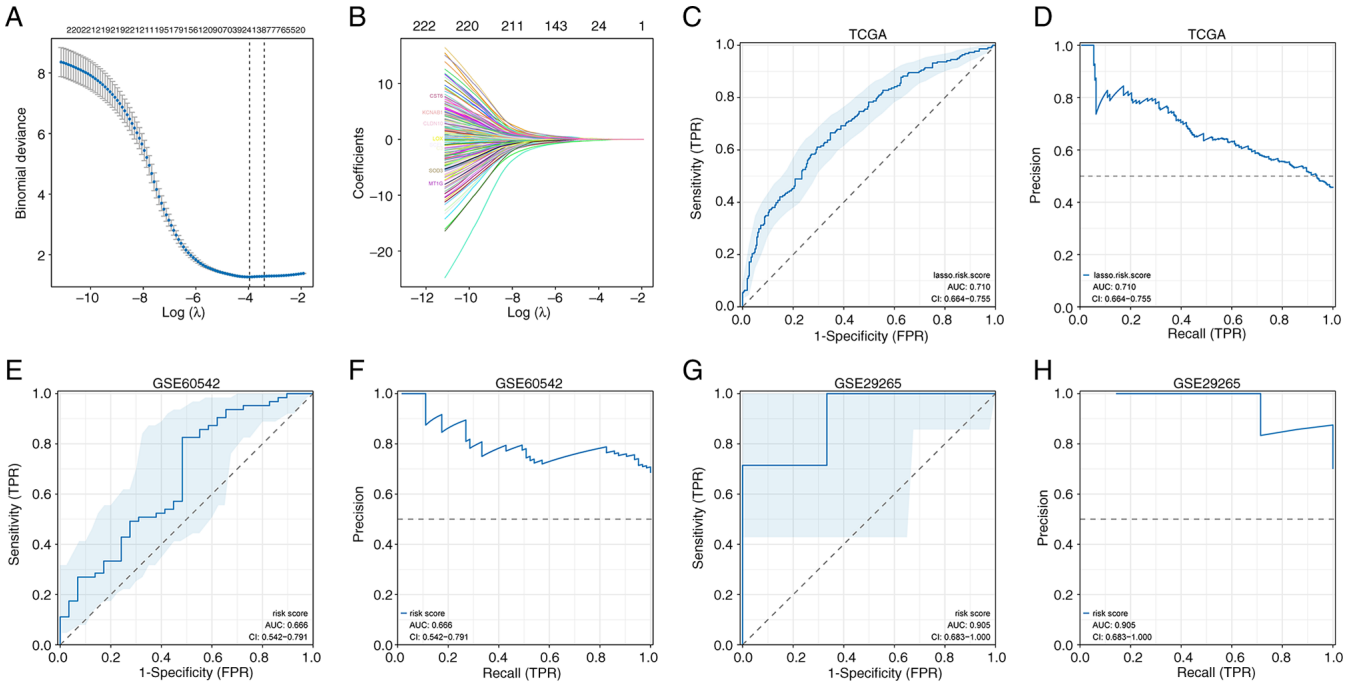

Figure 3. Development and validation of a diagnostic risk model for central lymph node metastasis based on *BRAF*-associated DEGs. (A and B) LASSO regression and cross-validation plots are used to identify the optimal gene signature. (C and D) ROC and precision-recall curves showing model performance in The Cancer Genome Atlas cohort (AUC=0.710). (E and F) External validation using GSE60542 dataset (AUC=0.666). (G and H) External validation using GSE29265 dataset (AUC=0.905), confirming model generalizability. DEGs, differentially expressed genes; LASSO, least absolute shrinkage and selection operator; ROC, receiver operating characteristic; AUC, area under the curve.

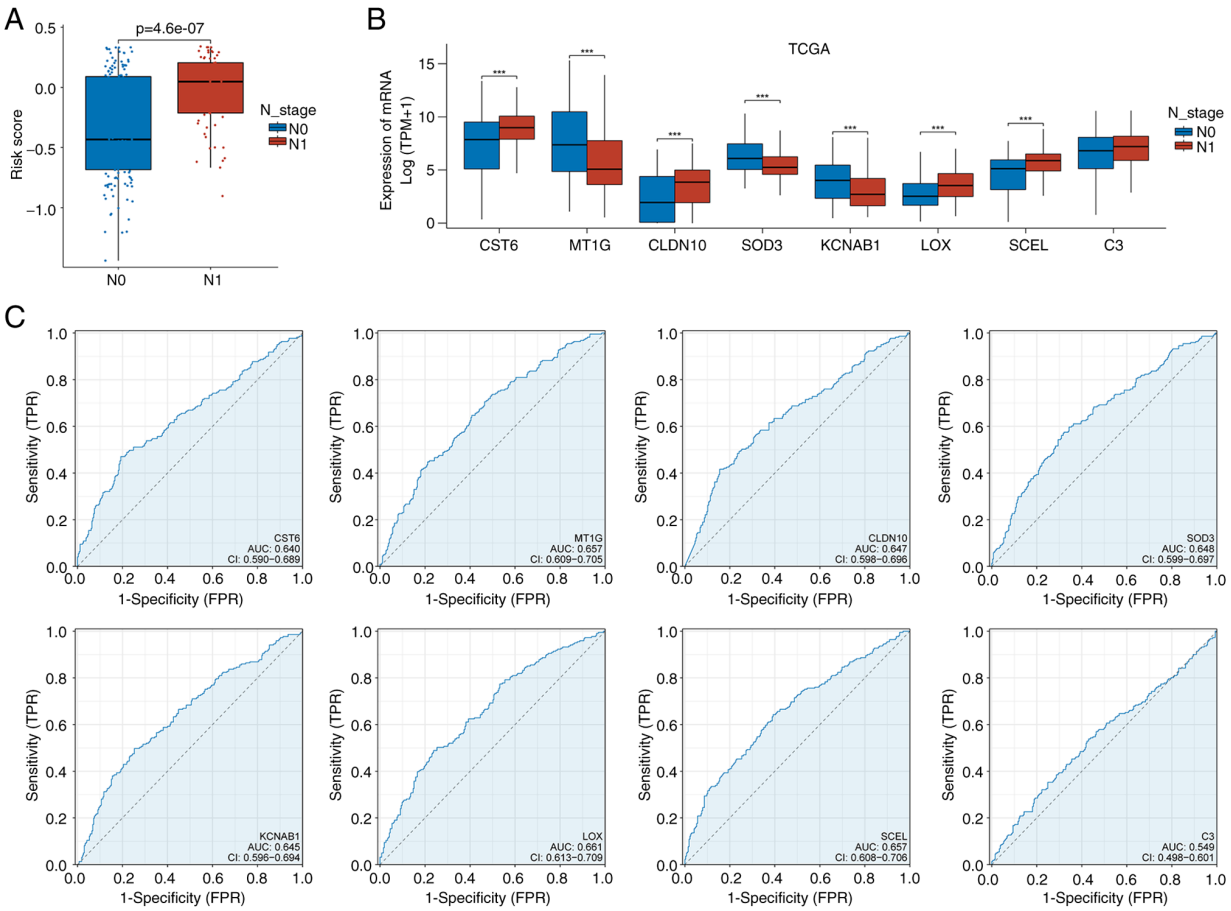

Figure 4. Expression and predictive value of model signature genes. (A) Boxplot comparing risk scores between CLNM-positive (N1) and -negative (N0) patients, showing higher scores in the metastatic group (P<0.001). (B) Heatmap of signature gene expression across CLNM subgroups. (C) ROC curves showing individual gene performance for CLNM prediction. ***P<0.001. CLNM, central lymph node metastasis; ROC, receiver operating characteristic.

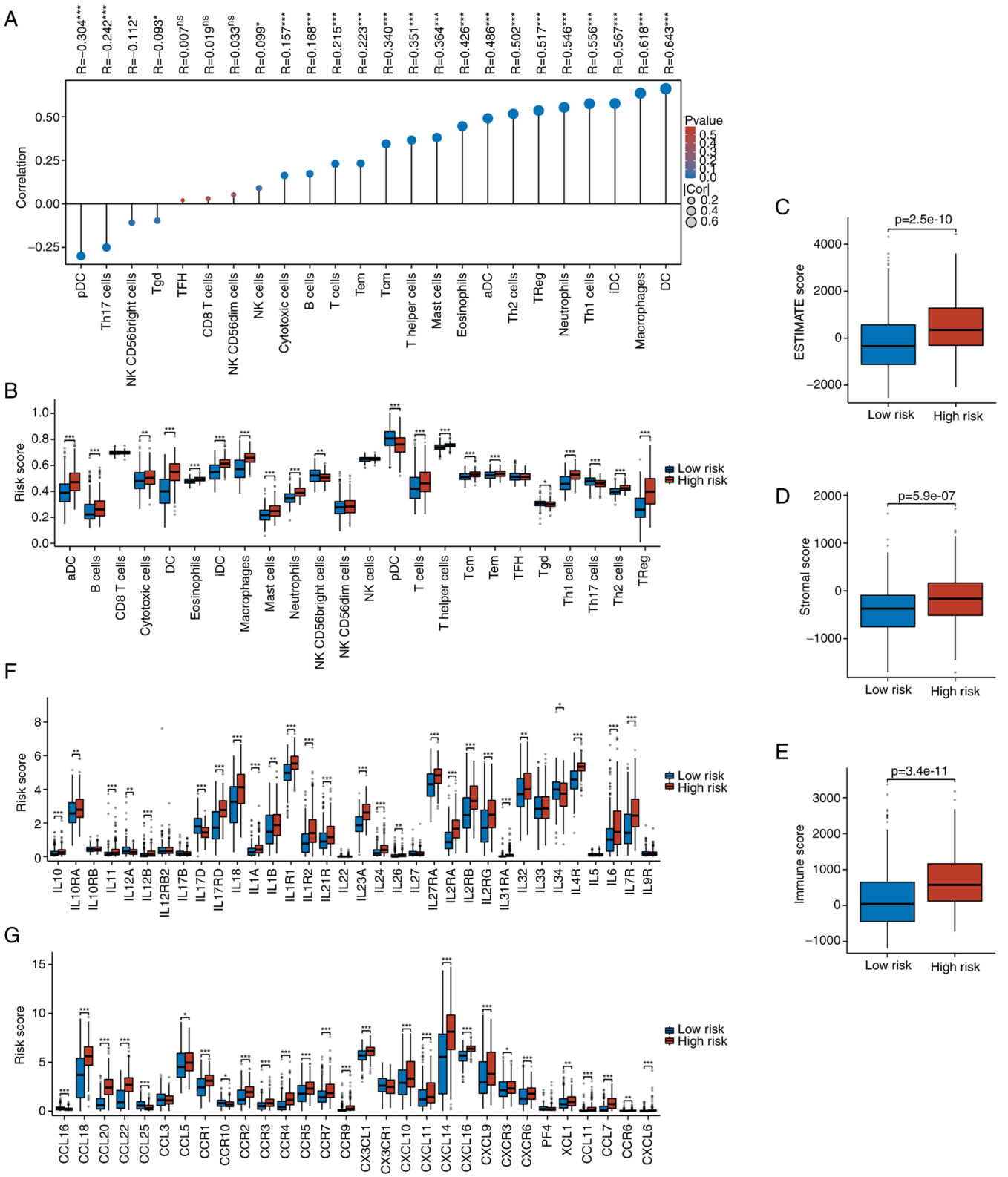

Figure 5. Association between risk score and tumor immune microenvironment in THCA. (A) Correlation heatmap of risk score with immune cell infiltration based on single-sample Gene Set Enrichment Analysis. (B) Comparison of immune cell type abundances between high- and low-risk groups. (C-E) Immune, stromal and ESTIMATE scores, indicating higher immune/stromal content in high-risk patients. (F and G) Differential expression of interleukins, chemokines and receptors, mostly elevated in high-risk patients. *P<0.05, **P<0.01, ***P<0.001. THCA, thyroid carcinoma.

Using these variables, a nomogram was constructed to estimate the probability of CLNM in patients with THCA (Fig. 7A). Calibration analysis showed a C-index of 0.769 (95% CI: 0.723-0.814), indicating favorable model fit (Fig. 7B). Further validation using a restricted cubic spline plot demonstrated overall significance and indicated a non-significant predominantly linear relationship between predictors and outcome (Fig. 7C). Decision curve analysis confirmed that the

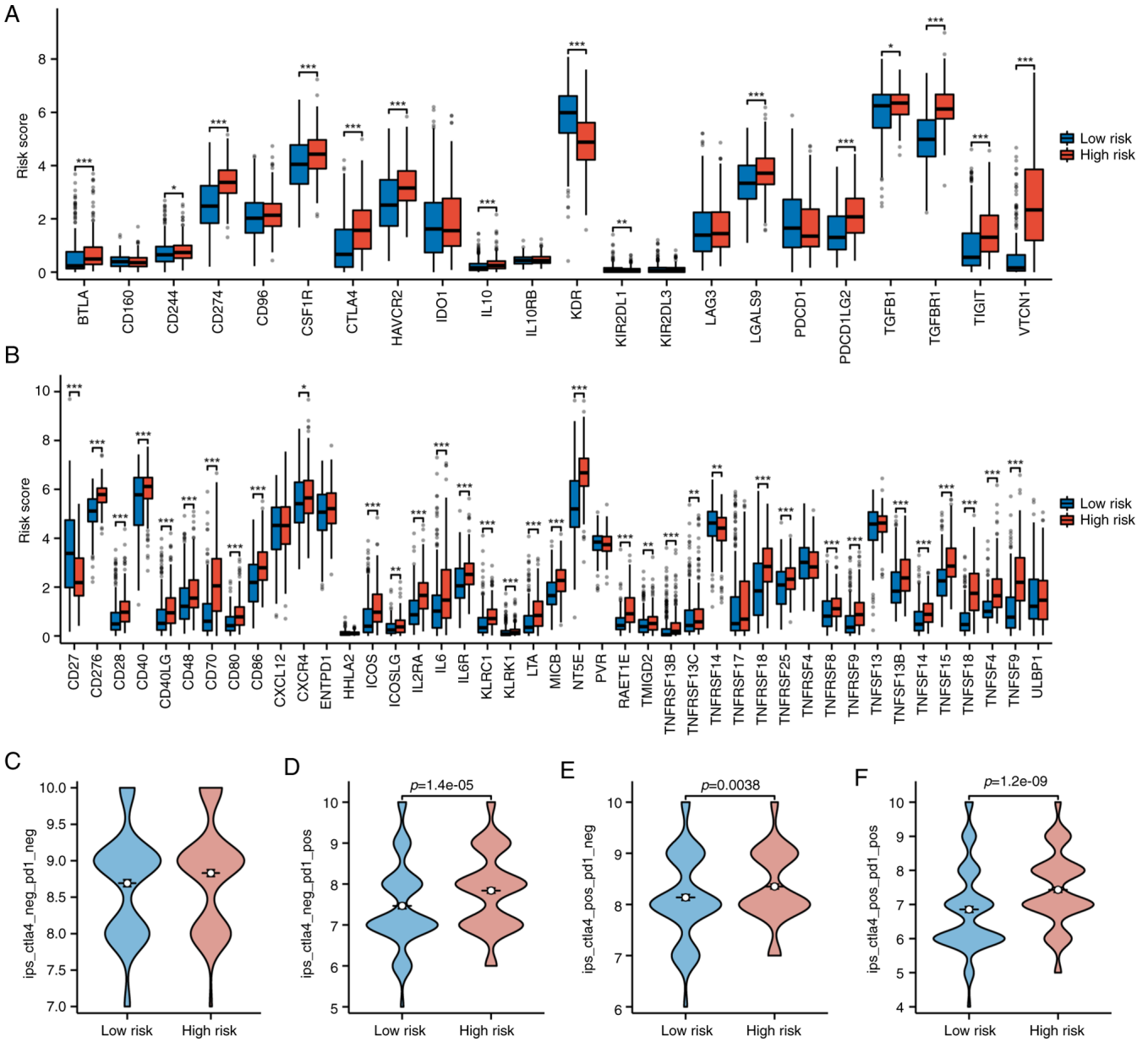

Figure 6. Immune checkpoint expression and IPS comparison between risk groups. (A and B) Differential expression of immune checkpoint inhibitors and stimulators in high- vs. low-risk patients, with upregulation in the high-risk group. (C-F) IPS analyses under four immunotherapy conditions (PD-1$^+$/CTLA4$^+$, PD-1+/CTLA4$^-$, PD-1$^-$/CTLA4$^+$, PD-1$^-$/CTLA4$^-$), indicating enhanced immunogenicity in high-risk patients. IPS, immunophenoscore; PD-1, programmed cell death protein 1; CTLA-4, cytotoxic T lymphocyte-associated protein 4. *P<0.05, **P<0.01, ***P<0.001.

combined model of age, T stage and risk score provided the highest net clinical benefit (Fig. 7D).

Predictive value of preoperative BRAF V600E mutation for CLNM. To evaluate the predictive value of *BRAF* V600E for CLNM in PTC, clinical data from 36 patients with cN0 PTC were analyzed who underwent preoperative ultrasound-guided central lymph node FNAC at Shunde Hospital, GUCM, between August 2022 and November 2023 were analyzed. After excluding four patients with insufficient samples, 32 patients were included, all of whom underwent total thyroidectomy (TT) and pCLND (Fig. 8A).

BRAF V600E mutation was detected in four patients using ARMS-PCR, three of whom had CLNM (Table III). Patients were categorized into non-mutation (n=28) and mutation (n=4) groups. CLNM rates were 32.1% in the non-mutation group and 75.0% in the mutation group (Fig. 8B). Although the mutation group showed higher CLNM incidence, the difference was not statistically significant. A Sankey diagram (Fig. 8C) illustrated that most *BRAF* V600E-positive patients experienced CLNM, whereas most non-mutation patients did not.

Postoperative BRAF V600E mutation and CLNM risk. A retrospective analysis of 222 PTC cases was performed to assess the association between *BRAF* V600E and CLNM risk. After excluding 42 cases lacking *BRAF* testing or lymph node dissection, 180 patients were analyzed, all of whom underwent TT with ipsilateral pCLND (Fig. 9A).

Patients were grouped by *BRAF* V600E status into non-mutation (n=100) and mutation (n=80) groups (Table IV).

Table II. Univariate and multivariate analyses of central lymph node metastasis status in patients with papillary thyroid carcinoma.

Characteristic	Total (n=424)	OR (95% CI) univariate analysis	P-value	OR (95% CI) multivariate analysis	P-value
Age, years					
>45	225	Reference		Reference	
≤45	199	1.664 (1.133-2.445)	0.009	2.032 (1.298-3.179)	0.002
Sex					
Male	112	Reference		Reference	
Female	312	0.612 (0.395-0.947)	0.027	0.716 (0.435-1.178)	0.188
Focus type					
Unifocal	227	Reference		Reference	
Multifocal	197	1.601 (1.090-2.352)	0.016	1.469 (0.898-2.404)	0.126
Location					
Right lobe	176	Reference		Reference	
Left lobe	152	1.343 (0.868-2.078)	0.186	1.250 (0.763-2.046)	0.376
Bilateral	77	2.281 (1.317-3.953)	0.003	1.723 (0.868-3.423)	0.120
Isthmus	19	1.895 (0.727-4.943)	0.191	1.504 (0.539-4.197)	0.436
T					
T1	124	Reference		Reference	
T2	131	1.659 (0.998-2.758)	0.051	1.902 (1.086-3.331)	0.024
T3	149	3.176 (1.930-5.228)	<0.001	2.709 (1.555-4.719)	<0.001
T4	20	11.472 (3.180-41.388)	<0.001	12.940 (3.309-50.602)	<0.001
Group					
Low	205	Reference		Reference	
High	219	4.613 (3.063-6.948)	<0.001	3.910 (2.518-6.071)	<0.001

Table III. Correlation between *BRAF* V600E mutation and CLNM in post-operative in patients with papillary thyroid carcinoma.

	Lymph node metastasis, n (%)	
Group	Yes	No
non-Mut (n=28)	9 (32.1)	19 (67.9)
Mut (n=4)	3 (75.0)	1 (25.0)

Representative IHC images of *BRAF* V600E expression in four patients are demonstrated in Fig. 9B, with additional details in Table V. CLNM occurred in 28.0% of non-mutation and 33.8% of mutation patients, with no statistically significant difference (Fig. 9C). A Sankey diagram (Fig. 9D) shows a higher proportion of CLNM in the *BRAF* V600E mutation group compared with the non-mutation group.

Discussion

The rising incidence of THCA is largely attributable to improved detection methods, yet overall mortality remains low, and numerous thyroid nodules exhibit indolent behavior (21). Nonetheless, LNM markedly increases recurrence and mortality risk, making its prediction and management a central clinical concern. In classical PTC, CLNM is particularly relevant to prognosis. Reported prevalence of CLNM ranges from 20-90%, while preoperative ultrasound demonstrates limited sensitivity, occasionally as low as 12.1% (22). In total, ~60% of patients with PTC are confirmed to have CLNM during initial surgery despite negative preoperative imaging (23), highlighting the need for reliable preoperative predictive models to better guide surgical decision-making.

Routine pCLND remains controversial. Critics argue that it offers limited survival or recurrence benefit while increasing postoperative complications. A total of ~14% of patients undergoing TT with pCLND develop temporary hypoparathyroidism, and 4% experience permanent hypoparathyroidism (24). The modest reduction in recurrence (0.66%) is counterbalanced by a 1.83% increase in temporary hypoparathyroidism (25), and risks of parathyroid and recurrent laryngeal nerve injury (26). Meta-analyses report permanent hypoparathyroidism at 1.1%, permanent recurrent laryngeal nerve injury at 0.5%, and recurrence at 2.8% in the pCLND group (27), with vocal cord paralysis ranging 3.28-27.8% (28). Taken together, these data highlight that indiscriminate pCLND may cause more harm than benefit, thereby emphasizing the potential utility of preoperative diagnostic models to refine indications for CLND and minimize morbidity.

The present study identified age, T stage and *BRAF* V600E mutation status as significant predictors of CLNM, consistent with established risk stratification frameworks. The ATA risk system guides postoperative management, particularly

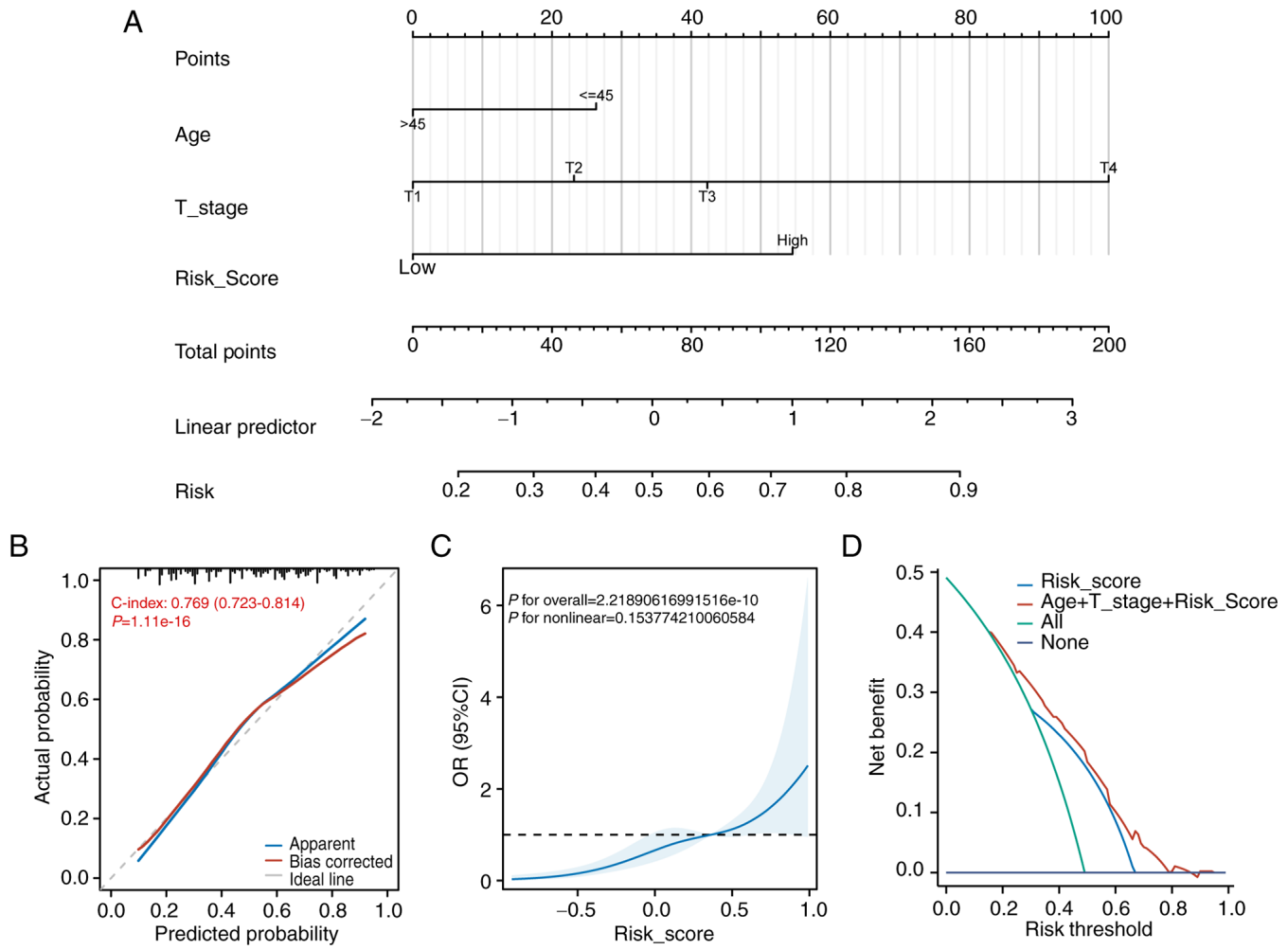

Figure 7. Construction and validation of a nomogram for predicting CLNM in papillary thyroid carcinoma. (A) Nomogram integrating age, T stage and risk score for individualized prediction of CLNM probability. (B) Calibration plot demonstrating agreement between predicted and observed probabilities (C-index=0.769). (C) Restricted cubic spline analysis confirming linear relationship between risk score and CLNM risk. (D) Decision curve analysis showing net clinical benefit of combined model compared with individual predictors. CLNM, central lymph node metastasis; CI, confidence interval.

for radioactive iodine therapy and follow-up intensity (5). CLNM is a key determinant in assigning intermediate or high ATA risk categories. Ghaznavi *et al* (29) demonstrated that integrating AJCC staging, ATA risk, and age refines disease-specific survival estimates, especially in younger patients with high-risk features. Building on this, our nomogram, incorporating preoperative variables (*BRAF* V600E, age and tumor size), provides an additional tool to stratify risk before surgery. Importantly, the model showed favorable calibration and discrimination in the TCGA cohort, with decision curve analysis confirming superior clinical benefit compared with individual predictors. Thus, preoperative *BRAF*-based models and postoperative ATA risk stratification may be complementary, together enabling more individualized treatment strategies. Importantly, our prognostic model did not include classical genes such as TERT or KRAS, consistent with recent literature (30), emphasizing the unique predictive value of *BRAF* V600E. Moreover, the LASSO-derived gene signature demonstrated strong performance, with external validation in GSE29265 achieving an AUC of 0.905.

The relationship between age, tumor size and CLNM remains debated. Some studies report no significant association (31), whereas others, including Ahn *et al* (32), identify age ≤45 years as an independent risk factor, consistent with the present findings. Tumor size is also recognized as a risk factor, though thresholds vary: ≥1 cm per Ahn *et al* (32) versus ≥0.25 cm per Yan *et al* (33). Our dataset included few nodules ≥4 cm, which may limit statistical accuracy. These discrepancies highlight the need for larger datasets to clarify cutoff values for more robust clinical applications.

Molecular insights have highlighted the significance of *BRAF* mutations in PTC. *BRAF* is the most frequently mutated gene in THCA, with V600E promoting cell proliferation and tumor aggressiveness (34,35). Preoperative detection of *BRAF* V600E informs surgical planning, recurrence risk stratification and potential I-131 therapy (36-38). The results of the present study confirmed that *BRAF* V600E-positive patients show higher recurrence and metastasis rates, supporting more intensive follow-up and, where appropriate, more aggressive management.

The link between *BRAF* V600E and CLNM, however, remains controversial. Xing *et al* (39,40) suggested that this mutation significantly increases the likelihood of CLNM in patients with PTC. In the present study, preoperative

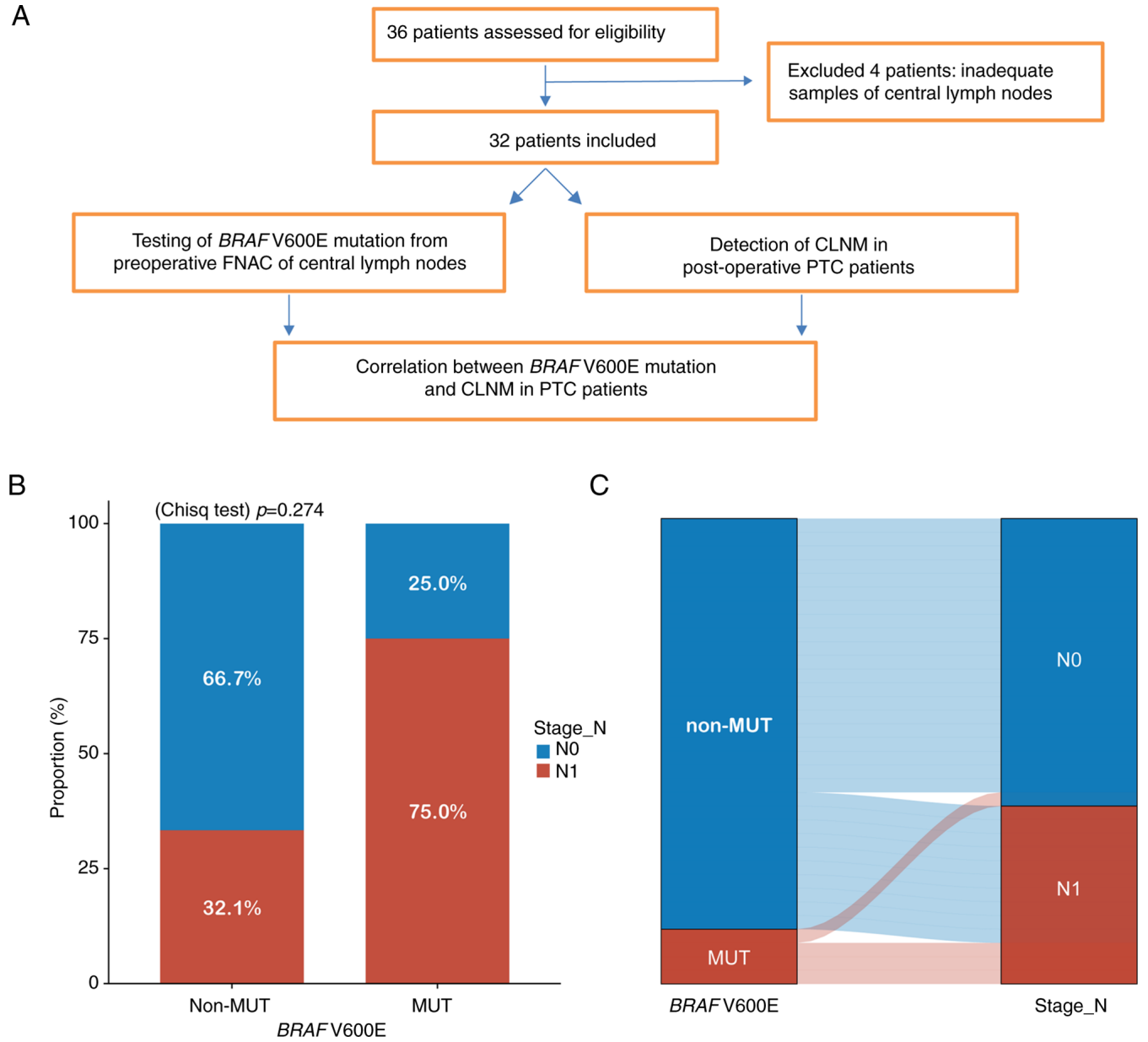

Figure 8. Predictive utility of preoperative *BRAF* V600E testing via FNAC. (A) Flowchart of patient inclusion and analysis for preoperative FNAC-based *BRAF* V600E detection. (B) Comparison of CLNM incidence in patients with and without *BRAF* V600E mutation, showing higher but non-significant risk in mutant group. (C) Sankey diagram illustrating CLNM distribution by *BRAF* mutation status. FNAC, fine-needle aspiration cytology; CLNM, central lymph node metastasis; PTC, papillary thyroid carcinoma.

FNAC with ARMS-PCR enabled detection of *BRAF* V600E in patients with cN0, suggesting potential utility in guiding prophylactic CLND. Further analysis of *BRAF* V600E-associated DEGs identified LOX and CST6 as potential mediators: LOX mediates extracellular matrix remodeling and metastasis (41-43), whereas CST6 may modulate the TME and metastatic potential (44). These genes could act as downstream or parallel mediators of *BRAF*-driven MAPK signaling, rationalizing their association with elevated CLNM risk.

Immune microenvironment analysis reinforced the clinical implications of our risk model. High-risk patients with THCA displayed a distinctive 'inflamed' immune phenotype, with substantial infiltration of DCs, macrophages, neutrophils, Th1/Th2 cells and Tregs, along with higher stromal and immune scores. This pattern, consistent with Xie *et al* (45), indicates an activated yet functionally constrained immune context. The broad upregulation of cytokines and chemokines, including immunosuppressive mediators such as IL-10 and TGF-β (46), together with increased expression of multiple immune checkpoint molecules (for example, PD-L1, CTLA-4, TIGIT and HAVCR2) (47), reflects T-cell exhaustion. Notably, IPS analysis suggested that high-risk patients may respond more favorably to immune checkpoint inhibitors, particularly combined PD-1/CTLA-4 blockade, suggesting that despite worse prognosis, they could derive substantial benefit from immunotherapy (48). Thus, the current findings not only delineate metastatic risk but also identify an immunological subset of patients potentially suited for targeted immunotherapies.

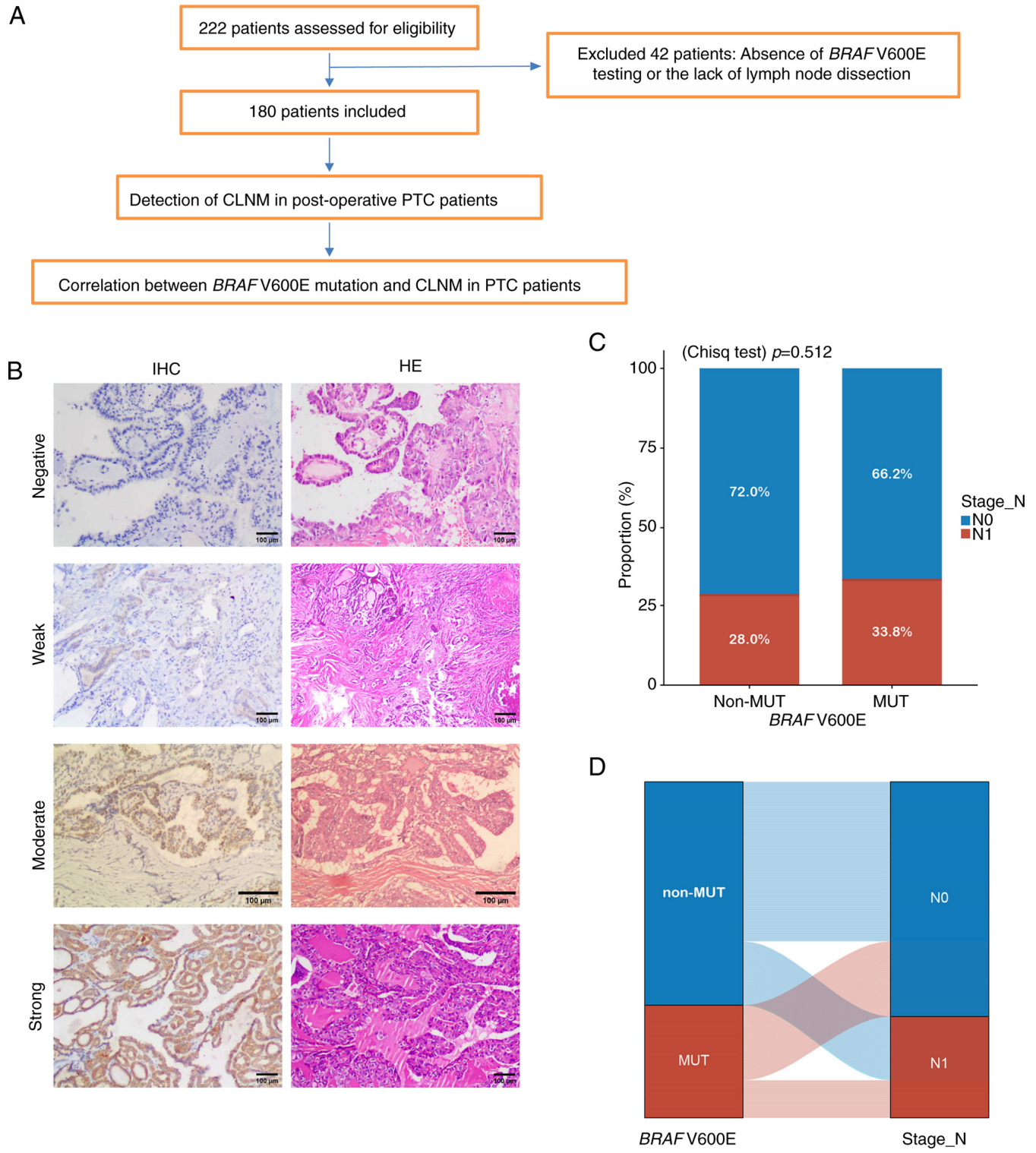

Figure 9. Postoperative IHC detection of *BRAF* V600E and CLNM association in PTC. (A) Flow diagram summarizing postoperative cohort selection. (B) Representative IHC images showed negative/weak/moderate/strong signal intensity of BRAF V600E expression (scale bar, 100 μm). (C) Bar chart comparing CLNM rates between BRAF-mutant and wild-type groups; higher incidence observed in mutant group without statistical significance. (D) Sankey diagram showing CLNM distribution according to postoperative *BRAF* mutation status. CLNM, central lymph node metastasis; PTC, papillary thyroid carcinoma; IHC, immunohistochemistry.

Several methodological and cohort-related limitations warrant consideration. Because of the limited volume of FNAC specimens, ARMS-PCR was used for BRAF V600E detection, whereas IHC was applied to postoperative samples owing to its practicality in routine pathology. As IHC is generally less sensitive than molecular methods such as PCR or NGS, this methodological difference may introduce false negatives, and the relatively small FNAC cohort, particularly the limited number of BRAF-positive cases, further reduced statistical power. In addition, the

Table IV. Clinical pathological characteristics of patients with papillary thyroid carcinoma (n=180) from Shunde Hospital of GUCM.

Characteristics	Overall no. (%)	*BRAF* V600E		P-value
		Mut, no. (%)	Non-mut, no. (%)	
n		80	100	
Sex, n (%)				0.480
Female	149 (82.8)	68 (37.8)	81 (45)	
Male	31 (17.2)	12 (6.7)	19 (10.6%)	
Age, n (%)				0.070
>45	81 (45)	42 (23.3)	39 (21.7)	
≤45	99 (55)	38 (21.1)	61 (33.9)	
T stage, n (%)				0.408[a]
T1	173 (96.1)	76 (42.2)	97 (53.9)	
T2	6 (3.3)	4 (2.2)	2 (1.1)	
T3	1 (0.6)	0 (0)	1 (0.6)	
N stage, n (%)				0.405
N1	55 (30.6)	27 (15)	28 (15.6)	
N0	125 (69.4)	53 (29.4)	72 (40)	
Primary neoplasm focus type, n (%)				0.506
Unifocal	137 (76.1)	59 (32.8)	78 (43.3)	
Multifocal	43 (23.9)	21 (11.7)	22 (12.2)	
Neoplasm location, n (%)				0.307[a]
Right	78 (43.3)	29 (16.1)	49 (27.2)	
Left	70 (38.9)	36 (20)	34 (18.9)	
Bilateral	27 (15)	12 (6.7)	15 (8.3)	
Isthmus	5 (2.8)	3 (1.7)	2 (1.1)	

Categorical data are presented as n (%). [a]P-values were obtained using Fisher's exact test (Monte Carlo method, based on 10,000 sampled tables) due to the presence of expected cell counts <5.

Table V. Clinical data and description of immunohistochemistry results.

Protein	Tissue	Age, years	Sex	Location	Quantity	Intensity
BRAF V600E	PTC	54	Female	-	-	Negative
BRAF V600E	PTC	35	Male	Cytoplasmic	40%	Weak
BRAF V600E	PTC	27	Male	Cytoplasmic	10%	Moderate
BRAF V600E	PTC	55	Female	Cytoplasmic	95%	

Strong PTC, papillary thyroid carcinoma.

detection rates of CLNM varied across cohorts (TCGA: BRAF+ 59.1% vs. BRAF- 35.7%, P<0.001; FNAC: 75% vs. 32.1%, P>0.05; IHC: 33.8% vs. 28.0%, P>0.05), which may reflect differences in detection techniques, population heterogeneity (Western vs. Chinese patients), and sample sizes; although the nomogram demonstrated acceptable discrimination in TCGA (AUC=0.710), its performance in external validation in GSE60542 was modest (AUC=0.666), underscoring the need for larger and more homogeneous cohorts as well as more sensitive molecular approaches (49). Finally, the nomogram of the present study was designed as a preoperative supplementary tool but was not directly compared with the ATA Risk Stratification System, an important limitation that should be addressed in future prospective studies.

Ultimately, these limitations highlight the need for future studies that incorporate larger and more homogeneous cohorts, employ sensitive molecular detection methods, and evaluate head-to-head comparisons with established clinical tools. Such efforts will facilitate the integration of molecularly informed

predictive models into routine practice, thereby improving preoperative risk stratification, surgical decision-making, and individualized management of THCA patients.

In summary, the present study identified age, T stage and *BRAF* V600E-associated high metastatic risk as independent predictors of CLNM in patients with PTC. The nomogram developed herein provides a practical visual tool for preoperative estimation of CLNM risk, supporting more precise surgical planning. For classical patients with PTC with TI-RADS ≥4a nodules and no radiologic evidence of cervical LNM, integrated assessment combining ultrasound-guided fine-needle aspiration with *BRAF* V600E mutation testing is recommended. This approach enables individualized risk stratification, informing surgical decision-making, reducing unnecessary procedures, and potentially improving patient outcomes and quality of life.

Acknowledgements

Not applicable.

Funding

The present study was supported by Self-funded Science and Technology Projects of Foshan (grant no. 2220001005113).

Availability of data and materials

The data generated and/or analyzed in the present study may be found in the TCGA database or at the following URL: (https://portal.gdc.cancer.gov).

Authors' contributions

JP and ZW contributed to conceptualization and study design and were involved in writing the original draft. YH performed the bioinformatic analysis and curated the data. RP was responsible for specimen collection and statistical analysis. ZF conducted lymph node punctures. JW performed the postoperative immunohistochemical analysis of thyroid and lymph nodes. ZW and YH confirm the authenticity of all the raw data. All authors reviewed the data, provided critical revisions, read and approved the final version of the manuscript.

Ethics approval and consent to participate

The study protocol was approved by the Ethics Committee of Shunde Hospital of Guangzhou University of Chinese Medicine (approval nos. KY2022066 and KY2023127; Foshan, China). Written informed consent was obtained from all participants for the use of their clinical and pathological data in the present research.

Patient consent for publication

Not applicable.

Competing interests

The authors declare that they have no competing interests.

References

1. Wiltshire JJ, Drake TM, Uttley L and Balasubramanian SP: Systematic review of trends in the incidence rates of thyroid cancer. Thyroid 26: 1541-1552, 2016.
2. Stonell R, Bannister P and Memon A: Changing epidemiology and trends in incidence of thyroid cancer in England, 1985-2019. Eur J Public Health 32 (Suppl 3): ckac130.053, 2022.
3. Yao F, Yang Z, Li Y, Chen W, Wu T, Peng J, Jiao Z and Yang A: Real-world evidence on the sensitivity of preoperative ultrasound in evaluating central lymph node metastasis of papillary thyroid carcinoma. Front Endocrinol (Lausanne) 13: 865911, 2022.
4. Zhang H: Interpretation of surgical update in 2018 Japanese clinical practice guidelines for thyroid tumors. Chin J Pract Surg 39: 5, 2019.
5. Haugen BR, Alexander EK, Bible KC, Doherty GM, Mandel SJ, Nikiforov YE, Pacini F, Randolph GW, Sawka AM, Schlumberger M, *et al*: 2015 American thyroid association management guidelines for adult patients with thyroid nodules and differentiated thyroid cancer: The American thyroid association guidelines task force on thyroid nodules and differentiated thyroid cancer. Thyroid 26: 1-133, 2016.
6. Filetti S, Durante C, Hartl D, Leboulleux S, Locati LD, Newbold K, Papotti MG and Berruti A; ESMO Guidelines Committee. Electronic address: clinicalguidelines@esmo.org: Thyroid cancer: ESMO clinical practice guidelines for diagnosis, treatment and follow-up†. Ann Oncol 30: 1856-1883, 2019.
7. Han L and Xu H: China anti-cancer association guidelines for holistic integrative management of thyroid cancer (2022 abridged version). Chin J Clin Oncol 50: 325-330, 2023.
8. Haddad RI, Bischoff L, Ball D, Bernet V, Blomain E, Busaidy NL, Campbell M, Dickson P, Duh QY, Ehya H, *et al*: Thyroid carcinoma, version 2.2022, NCCN clinical practice guidelines in oncology. J Natl Compr Canc Netw 20: 925-951, 2022.
9. Zhao W, You L, Hou X, Chen S, Ren X, Chen G and Zhao Y: The effect of prophylactic central neck dissection on locoregional recurrence in papillary thyroid cancer after total thyroidectomy: A systematic review and meta-analysis: pCND for the locoregional recurrence of papillary thyroid cancer. Ann Surg Oncol 24: 2189-2198, 2017.
10. Yeh MW, Bauer AJ, Bernet VA, Ferris RL, Loevner LA, Mandel SJ, Orloff LA, Randolph GW and Steward DL; American Thyroid Association Surgical Affairs Committee Writing Task Force: American thyroid association statement on preoperative imaging for thyroid cancer surgery. Thyroid 25: 3-14, 2015.
11. Zhao H and Li H: Meta-analysis of ultrasound for cervical lymph nodes in papillary thyroid cancer: Diagnosis of central and lateral compartment nodal metastases. Eur J Radiol 112: 14-21, 2019.
12. Dai Q, Tao Y, Liu D, Zhao C, Sui D, Xu J, Shi T, Leng X and Lu M: Ultrasound radiomics models based on multimodal imaging feature fusion of papillary thyroid carcinoma for predicting central lymph node metastasis. Front Oncol 13: 1261080, 2023.
13. Seo YL, Yoon DY, Lim KJ, Cha JH, Yun EJ, Choi CS and Bae SH: Locally advanced thyroid cancer: Can CT help in prediction of extrathyroidal invasion to adjacent structures? AJR Am J Roentgenol 195: W240-W244, 2010.
14. Zou Y, Zhang H, Li W, Guo Y, Sun F, Shi Y, Gong Y, Lu X, Wang W and Xia S: Prediction of ipsilateral lateral cervical lymph node metastasis in papillary thyroid carcinoma: A combined dual-energy CT and thyroid function indicators study. BMC Cancer 21: 221, 2021.
15. Attia AS, Hussein M, Issa PP, Elnahla A, Farhoud A, Magazine BM, Youssef MR, Aboueisha M, Shama M, Toraih E and Kandil E: Association of $BRAF^{V600E}$ mutation with the aggressive behavior of papillary thyroid microcarcinoma: A meta-analysis of 33 studies. Int J Mol Sci 23: 15626, 2022.
16. Parvathareddy SK, Siraj AK, Ahmed SO, DeVera F, Al-Sobhi SS, Al-Dayel F and Al-Kuraya KS: Risk factors for central lymph node metastases and benefit of prophylactic central lymph node dissection in middle eastern patients with cN0 papillary thyroid carcinoma. Front Oncol 11: 819824, 2022.
17. Hlozek J, Pekova B, Rotnágl J, Holý R and Astl J: Genetic changes in thyroid cancers and the importance of their preoperative detection in relation to the general treatment and determination of the extent of surgical intervention-A review. Biomedicines 10: 1515, 2022.
18. Yu G, Wang LG, Han Y and He QY: clusterProfiler: An R package for comparing biological themes among gene clusters. OMICS 16: 284-287, 2012.

19. Bindea G, Mlecnik B, Tosolini M, Kirilovsky A, Waldner M, Obenauf AC, Angell H, Fredriksen T, Lafontaine L, Berger A, *et al*: Spatiotemporal dynamics of intratumoral immune cells reveal the immune landscape in human cancer. Immunity 39: 782-795, 2013.
20. Yoshihara K, Shahmoradgoli M, Martínez E, Vegesna R, Kim H, Torres-Garcia W, Treviño V, Shen H, Laird PW, Levine DA, *et al*: Inferring tumour purity and stromal and immune cell admixture from expression data. Nat Commun 4: 2612, 2013.
21. Li N, Du XL, Reitzel LR, Xu L and Sturgis EM: Impact of enhanced detection on the increase in thyroid cancer incidence in the United States: Review of incidence trends by socioeconomic status within the surveillance, epidemiology, and end results registry, 1980-2008. Thyroid 23: 103-110, 2013.
22. Park CH, Song CM, Ji YB, Pyo JY, Yi KJ, Song YS, Park YW and Tae K: Significance of the extracapsular spread of metastatic lymph nodes in papillary thyroid carcinoma. Clin Exp Otorhinolaryngol 8: 289-294, 2015.
23. Gao L, Wang J, Jiang Y, Gao Q, Wang Y, Xi X and Zhang B: The number of central lymph nodes on preoperative ultrasound predicts central neck lymph node metastasis in papillary thyroid carcinoma: A prospective cohort study. Int J Endocrinol 2020: 2698659, 2020.
24. Ywata de Carvalho A, Chulam TC and Kowalski LP: Long-term results of observation vs prophylactic selective level VI neck dissection for papillary thyroid carcinoma at a cancer center. JAMA Otolaryngol Head Neck Surg 141: 599-606, 2015.
25. Yang J, Han Y, Min Y, Chen C, Chen J, Xiang K, Liao J, Feng Y, Hu D and Yin G: Prophylactic central neck dissection for cN0 papillary thyroid carcinoma: Is there any difference between western countries and China? A systematic review and meta-analysis. Front Endocrinol (Lausanne) 14: 1176512, 2023.
26. Pereira JA, Jimeno J, Miquel J, Iglesias M, Munné A, Sancho JJ and Sitges-Serra A: Nodal yield, morbidity, and recurrence after central neck dissection for papillary thyroid carcinoma. Surgery 138: 1095-1101, 2005.
27. Liu LS, Liang J, Li JH, Liu X, Jiang L, Long JX, Jiang YM and Wei ZX: The incidence and risk factors for central lymph node metastasis in cN0 papillary thyroid microcarcinoma: A meta-analysis. Eur Arch Otorhinolaryngol 274: 1327-1338, 2017.
28. Enomoto K, Uchino S, Watanabe S, Enomoto Y and Noguchi S: Recurrent laryngeal nerve palsy during surgery for benign thyroid diseases: Risk factors and outcome analysis. Surgery 155: 522-528, 2014.
29. Ghaznavi SA, Ganly I, Shaha AR, English C, Wills J and Tuttle RM: Using the American thyroid association risk-stratification system to refine and individualize the American joint committee on cancer eighth edition disease-specific survival estimates in differentiated thyroid cancer. Thyroid 28: 1293-1300, 2018.
30. Ji J and Shi X: Gene mutations as predictors of central lymph mode metastasis in cN0 PTC: A meta-analysis. Clin Genet 105: 130-139, 2024.
31. Khan H, Ullah H and Nabavi SM: Mechanistic insights of hepatoprotective effects of curcumin: Therapeutic updates and future prospects. Food Chem Toxicol 124: 182-191, 2019.
32. Ahn BH, Kim JR, Jeong HC, Lee JS, Chang ES and Kim YH: Predictive factors of central lymph node metastasis in papillary thyroid carcinoma. Ann Surg Treat Res 88: 63-68, 2015.
33. Yan H, Zhou X, Jin H, Zheng M, Ming X, Wang R and Liu J: A study on central lymph node metastasis in 543 cN0 papillary thyroid carcinoma patients. Int J Endocrinol 2016: 1878194, 2016.
34. Choi EK, Chong A, Ha JM, Jung CK, O JH and Kim SH: Clinicopathological characteristics including BRAF V600E mutation status and PET/CT findings in papillary thyroid carcinoma. Clin Endocrinol (Oxf) 87: 73-79, 2017.
35. Lasolle H, Schiavo A, Tourneur A, Gillotay P, de Faria da Fonseca B, Ceolin L, Monestier O, Aganahi B, Chomette L, Kizys MML, *et al*: Dual targeting of MAPK and PI3K pathways unlocks redifferentiation of Braf-mutated thyroid cancer organoids. Oncogene 43: 155-170, 2024.
36. Song Y, Xu G, Ma T, Zhu Y, Yu H, Yu W, Wei W, Wang T and Zhang B: Utility of a multigene testing for preoperative evaluation of indeterminate thyroid nodules: A prospective blinded single center study in China. Cancer Med 9: 8397-8405, 2020.
37. Yang K, Wang H, Liang Z, Liang J, Li F and Lin Y: BRAFV600E mutation associated with non-radioiodine-avid status in distant metastatic papillary thyroid carcinoma. Clin Nucl Med 39: 675-679, 2014.
38. Cheng W, Liu R, Zhu G, Wang H and Xing M: Robust thyroid gene expression and radioiodine uptake induced by simultaneous suppression of BRAF V600E and histone deacetylase in thyroid cancer cells. J Clin Endocrinol Metab 101: 962-971, 2016.
39. Xing M, Alzahrani AS, Carson KA, Shong YK, Kim TY, Viola D, Elisei R, Bendlová B, Yip L, Mian C, *et al*: Association between BRAF V600E mutation and recurrence of papillary thyroid cancer. J Clin Oncol 33: 42-50, 2015.
40. Xing M, Alzahrani AS, Carson KA, Viola D, Elisei R, Bendlova B, Yip L, Mian C, Vianello F, Tuttle RM, *et al*: Association between BRAF V600E mutation and mortality in patients with papillary thyroid cancer. JAMA 309: 1493-1501, 2013.
41. Boufraqech M, Patel D, Nilubol N, Powers A, King T, Shell J, Lack J, Zhang L, Gara SK, Gunda V, *et al*: Lysyl oxidase is a key player in BRAF/MAPK pathway-driven thyroid cancer aggressiveness. Thyroid 29: 79-92, 2019.
42. Jolly LA, Novitskiy S, Owens P, Massoll N, Cheng N, Fang W, Moses HL and Franco AT: Fibroblast-mediated collagen remodeling within the tumor microenvironment facilitates progression of thyroid cancers driven by BrafV600E and Pten loss. Cancer Res 76: 1804-1813, 2016.
43. Liu H, Sun X, Dong B, Zhang J, Zhang J, Gu Y, Chen L, Pang X, Ye J, Wang X and Rong Z: Systematic characterisation and analysis of lysyl oxidase family members as drivers of tumour progression and multiple drug resistance. J Cell Mol Med 29: e70536, 2025.
44. Oler G, Camacho CP, Hojaij FC, Michaluart P Jr, Riggins GJ and Cerutti JM: Gene expression profiling of papillary thyroid carcinoma identifies transcripts correlated with BRAF mutational status and lymph node metastasis. Clin Cancer Res 14: 4735-4742, 2008.
45. Xie Z, Li X, He Y, Wu S, Wang S, Sun J, He Y, Lun Y and Zhang J: Immune cell confrontation in the papillary thyroid carcinoma microenvironment. Front Endocrinol (Lausanne) 11: 570604, 2020.
46. Ferrari SM, Fallahi P, Galdiero MR, Ruffilli I, Elia G, Ragusa F, Paparo SR, Patrizio A, Mazzi V, Varricchi G, *et al*: Immune and inflammatory cells in thyroid cancer microenvironment. Int J Mol Sci 20: 4413, 2019.
47. Kurachi M: $CD8^+$ T cell exhaustion. Semin Immunopathol 41: 327-337, 2019.
48. Zander AD, Erbe R, Liu Y, Jin A, Hyun SW, Mukhopadhyay S, Terdich B, Rosasco MG, Patel N, Mahon BM, *et al*: Development and validation of the immune profile score (IPS), a novel multiomic algorithmic assay for stratifying outcomes in a real-world cohort of patients with advanced solid cancer treated with immune checkpoint inhibitors. J Immunother Cancer 13: e011363, 2025.
49. Fu G, Chazen RS, MacMillan C and Witterick IJ: Development of a molecular assay for detection and quantification of the BRAF variation in residual tissue from thyroid nodule fine-needle aspiration biopsy specimens. JAMA Netw Open 4: e2127243, 2021.